Journal of Materials Chemistry A

ROYAL SOCIETY OF CHEMISTRY

PAPER

View Article Online
View Journal

Cite this: DOI: 10.1039/d4ta07622b

Ultra-flexible organic solar cells based on eco-friendly cellulose substrate with efficiency approaching 19%†

Zheng Xiao, Jian Liu, Xin Chen, Zhaochen Suo, Xiangjian Cao, Nuo Xu, Zhaoyang Yao, Chenxi Li, Xiangjian Wan * and Yongsheng Chen *

Received 25th October 2024
Accepted 10th December 2024

DOI: 10.1039/d4ta07622b

rsc.li/materials-a

Flexible organic solar cells (OSCs), especially ultra-flexible OSCs, show great potential for applications in wearable devices and related fields. However, improving their performance remains a significant challenge in the flexible OSC field. Despite its importance as a key component in flexible devices, the flexible substrate has received relatively little attention, which indeed hinders further improvement in flexible OSC performance. In this study, we developed an eco-friendly, ultra-flexible substrate with high solvent resistance, outstanding mechanical durability, and excellent light transmittance by constructing an ethoxylated trimethylolpropane triacrylate (ETPTA) polymer network within an ethyl cellulose (EC) film. OSCs fabricated on this substrate achieved a record power conversion efficiency (PCE) of 18.71% and a high power-per-weight ratio of 30.04 W g^{-1}. Furthermore, the ultra-flexible OSCs demonstrated excellent mechanical resilience, retaining 93.47% of their initial efficiency after 10 000 bending cycles at a bending radius of 1 mm.

Introduction

Flexible organic solar cells (OSCs) demonstrate significant potential for applications in human health monitoring, the Internet of Things, and other fields.[1–5] Ultra-flexible OSCs (with thicknesses ≤ 10 μm) offer enhanced mechanical compliance and deformability, making them ideal for adapting to uneven surfaces and promising for future practical applications in wearable electronics, aerospace equipment, and robotics.[6–9] A key component in flexible OSCs is the flexible transparent electrode, which critically influences the overall performance of these devices.[10–12] Over the past decade, considerable attention has been devoted to developing and optimizing conductive layers, such as silver nanowires (AgNWs),[13–15] conductive polymers,[16,17] and carbon materials,[18,19] to replace the rigid indium tin oxide (ITO). However, the importance of the flexible substrate has often been overlooked.[20,21] In fact, the substrate is a crucial element of flexible OSCs, significantly impacting flexibility, optical transmittance, mechanical robustness, and processing temperature.[22–25] Commonly used flexible substrates like PET[26] and PEN[27,28] are limited by their low glass transition temperatures (T_g),[29–31] which restrict their thermal tolerance. Polyimide (PI), with its excellent mechanical properties and thermal stability, is the most widely used substrate for ultra-flexible devices.[32,33] However, the high preparation temperature (generally over 200 °C) of PI limits its application scenarios, and its relatively low transmittance in the visible light region hinders the PCEs of flexible OSCs.[34,35] Additionally, the long degradation process of the above three plastic substrates in natural environments poses sustainability challenges, leading to resource and energy waste.[36–38] Therefore, there is an urgent need to develop next-generation sustainable flexible substrates suitable for highly efficient flexible OSCs.

In recent years, cellulose-based flexible substrates have attracted attention for use in electronic devices. Thin films made from cellulose are lightweight, transparent, heat-stable, and have shown great potential in flexible electronic devices and OSCs.[39] However, most flexible OSCs based on cellulose substrates have exhibited low efficiencies, primarily due to the poor performance of cellulose substrate-based flexible electrodes.[31,40,41] To our knowledge, it is worthy to note that no ultra-flexible OSCs using cellulose-based substrates have been reported, as current cellulose substrates fail to meet the stringent requirements for ultra-flexible electrodes.[42,43] High-performance ultra-flexible transparent electrodes are essential for ultra-flexible OSCs, placing higher demands on both the substrate and electrodes.[44,45] Firstly, the flexible substrate should have good solvent tolerance to prevent damage during the layer-by-layer solution processing of OSC devices.[46–48] Secondly, the flexible substrate must possess excellent mechanical properties.[49,50] Lastly, the conductive layer should

State Key Laboratory of Elemento-Organic Chemistry, Key Laboratory of Functional Polymer Materials, College of Chemistry, Renewable Energy Conversion and Storage Center (RECAST), Nankai University, Tianjin 300071, China. E-mail: xjwan@nankai.edu.cn; yschen99@nankai.edu.cn

† Electronic supplementary information (ESI) available: Experimental details. See DOI: https://doi.org/10.1039/d4ta07622b

have high transmittance, good conductivity, low surface roughness, and excellent durability.[51] Silver nanowires (AgNWs), known for their numerous advantages, are commonly used as conductive layers in ultra-flexible electrodes. There are two widely used methods for preparing ultra-flexible electrode based on AgNWs: the direct preparation method and the embedded method.[52] The first involves preparing the electrode directly on a flexible substrate adhered to a rigid support, followed by peeling off the entire OSC after device fabrication.[53,54] This method is simple and convenient but presents challenges in controlling the surface roughness of the silver nanowires.[55] The second, the embedded method, involves first coating AgNWs onto a hard substrate, preparing the flexible substrate on top, and then transferring the embedded electrode to another rigid substrate for device fabrication.[56] Although this method results in lower surface roughness, the ultra-flexible electrode is prone to wrinkling, complicating subsequent device preparation.[57–59]

In this study, we developed an ultra-flexible electrode using an ethyl cellulose (EC) composite substrate combined with AgNWs as the conductive layer. To enhanced the mechanical properties and solvent resistance of the EC substrate, ethoxylated trimethylolpropane triacrylate (ETPTA) was introduced as a crosslinker. Upon UV illumination, polymer networks form within the composite film, significantly enhancing the solvent resistance and reducing the surface roughness of the flexible substrate. The resulting composite film also exhibits excellent mechanical robustness and flexibility. We then prepared ultra-flexible transparent electrodes with high conductivity and transmittance, and exceptional bending resistance by depositing AgNWs onto the EC@ETPTA flexible substrate. Ultimately, we achieved an ultra-flexible OSC with a PCE of 18.71% and a power-to-weight ratio of 30.04 W g^{-1}, setting a new record for PCE in flexible OSCs.[60,61] Moreover, these ultra-flexible devices demonstrate outstanding mechanical properties, retaining 93.47% of their efficiency after 10 000 bends at a radius of 1 mm.

Results and discussion

Pure EC film exhibits poor resistance to organic solvents, swelling or shrinking when exposed to common solvents like methanol, ethanol, chloroform, and chlorobenzene, which are widely used in fabricating OSC interfaces and active layers. To address this issue, we incorporated ethoxylated trimethylolpropane triacrylate (ETPTA) as a crosslinker into the EC film to create a composite film, EC@ETPTA. Fig. 1a illustrates the formation of polymer networks within the composite film after UV illumination, which is confirmed by enhanced mechanical strength and solvent resistance. As shown in Fig. 1b, the film's tensile strength increased from 42.89 MPa to 84.96 MPa as the ETPTA content was raised from 0% to 30%. Notably, the elongation at break for EC@ETPTA containing 10% and 20% ETPTA also improved, with a particularly significant increase at 20% ETPTA, where the elongation at break doubled compared to pure EC. The thermal expansion coefficients (TEC) of the EC and EC@ETPTA (20%) films were measured using static Thermal Mechanical Analysis (TMA). The EC film show a low TEC of 50.73 $\times$ 10^{-6} K^{-1} from 25 to 100 °C in nitrogen atmosphere. However, it underwent significant deformation at 112 °C due to softening. In contrast, the TEC of EC@ETPTA film increased to 127.90 $\times$ 10^{-6} K^{-1}, but the softening phenomenon was eliminated (Fig. S1†).

The solvent resistance of the composite film with 20% ETPTA was evaluated using the established method, which involved wiping the film surface with a cotton swab soaked with organic solvents such as methanol, butanol, and chloroform.[62–64] As shown in Fig. S2 and S3,† the pure EC film was easily scratched off, whereas the EC@ETPTA film remained intact, indicating the good solvent resistance of the composite film. To measure the gel fraction, the EC composite films with different ETPTA contents were immersed in n-butanol at room temperature for 24 hours. As shown in Fig. S4,† the residual weight of EC@ETPTA films with initial ETPTA content of 10%, 20% and 30% in *n*-butanol is 93.55%, 96.02% and 97.53%, respectively. Furthermore, EC@ETPTA films containing 20% ETPTA were immersed in various solvents commonly used for FOSCs at room temperature for 24 hours, including ethanol (EA), methanol (MeOH), chloroform (CF), *o*-xylene (OX), and water (H_2O). The residual weights were 97.21%, 96.51%, 94.88%, 99.62%, and 100.00%, respectively, demonstrating that the composite film exhibits excellent resistance to solvents.

As shown in Fig. 1c, the FTIR spectrum of the ETPTA monomer before UV treatment displays two characteristic peaks at 1635 cm^{-1} and 820 cm^{-1}, corresponding to the C=C stretching and twisting vibrations, respectively, in the acrylate group. After the UV-curing reaction, these two peaks disappear in the FTIR spectrum of the EC@ETPTA film, indicating that the ETPTA monomer has fully crosslinked, forming a three-dimensional polymer network within the composite film. To further investigate the distribution of the ETPTA polymer network in the EC@ETPTA films, atomic force microscopy-infrared spectroscopy (AFM-IR) was employed. As shown in Fig. 1d, the infrared vibration signal of C=O at 1740 cm^{-1}, which is absent in EC but present in ETPTA polymer (Fig. S5†), allowed for easy distinction between the two components in the AFM-IR measurements. The AFM-IR images reveal that ETPTA and EC are well-mixed, forming uniform EC@ETPTA films. This uniform dispersion is further confirmed by the smaller root-mean-square (RMS) roughness of EC@ETPTA (0.79 nm) compared to that of pure EC (1.59 nm) (Fig. 1e).

Due to the high transmittance of the ETPTA polymer and EC film (Fig. S6†), the prepared EC@ETPTA composite film, at a thickness of 8 μm (Fig. S8†), exhibits an average transmittance as high as 91% across a broad wavelength range of 400 to 1000 nm (Fig. 2a). Notably, this composite film can be easily prepared on a large area using the doctor-blading method, as demonstrated by the 23 cm $\times$ 13 cm EC@ETPTA film shown in Fig. 2a and S9.† Using this EC composite film, we prepared an ultra-flexible transparent electrode by coating a uniformly distributed layer of AgNWs on it (Fig. S10†), following our previously reported method. As shown in Fig. 2b, the ultra-flexible electrode, EC@ETPTA/AgNWs, demonstrates an average transmittance of over 88.01% within the 400 to 1000 nm

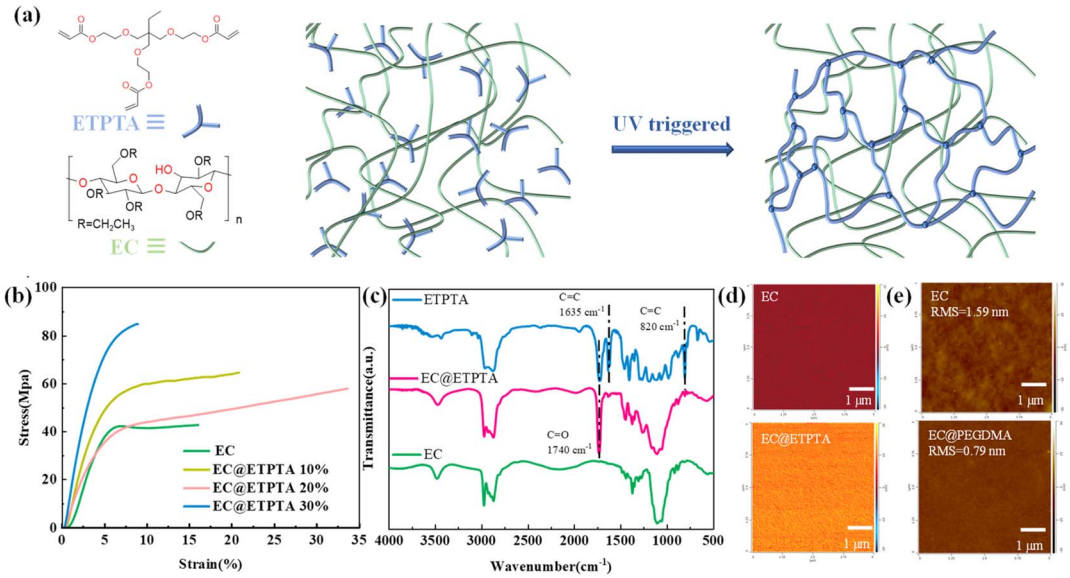

Fig. 1 (a) Schematic illustrations of EC@ETPTA film. (b) The tensile stress–strain curves of pure EC and EC@ETPTA. (c) FT-IR spectra of EC, ETPTA and EC@ETPTA. (d) AFM-IR images (recorded at 1740 cm^{-1} corresponding to the C=O stretching vibration). (e) AFM images of pure EC and EC@ETPTA films.

wavelength range, with a peak transmittance of 88.92% at 550 nm, and a low sheet resistance of 21.04 Ω □$^{-1}$, comparable to that of commercial glass/ITO electrodes. In contrast, commercial flexible electrodes such as PEN/ITO and PET/ITO exhibit significantly lower transparency, especially in the near-infrared range.

In addition to achieving high transmittance and low sheet resistance (R_{sh}), flexibility under bending stress is also critical for ultra-flexible transparent electrodes. The bending durability of these electrodes was assessed by monitoring the ratio of the sheet resistance (R_{sh}) during bending cycles at different bending radii. Fig. 2c illustrates the normalized sheet resistance

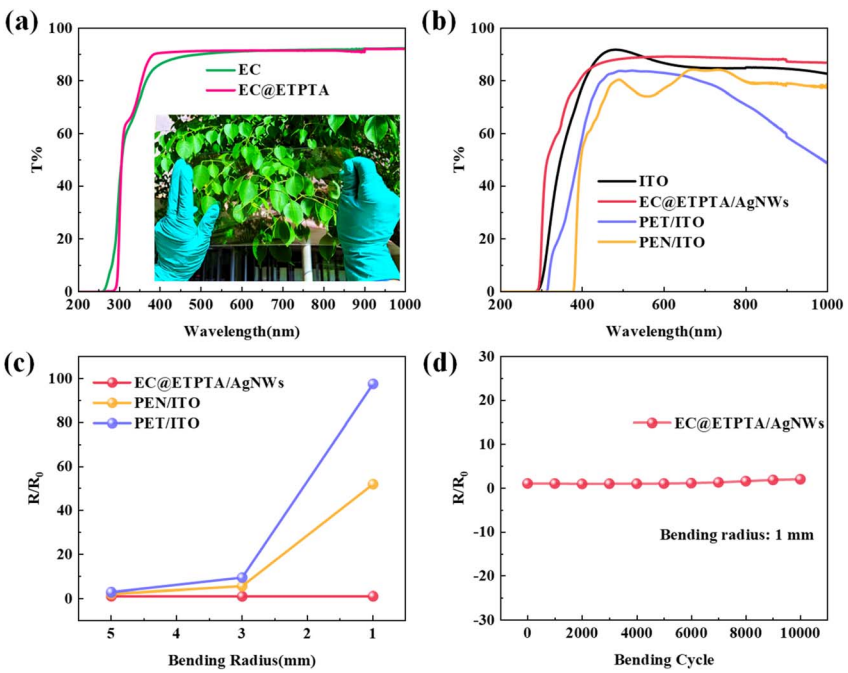

Fig. 2 (a) Transmittance spectra of EC and EC@ETPTA films and photo of EC@ETPTA film with a size of 23 cm × 13 cm. (b) Transmittance spectra of the glass/ITO, PET/ITO, PEN/ITO and EC@ETPTA/AgNWs electrodes. (c) The normalized square resistance of the EC@ETPTA/AgNWs electrode, PEN/ITO and PET/ITO after 1000 bending tests with different radii. (d) The normalized square resistances of the EC@ETPTA/AgNWs electrode during 10 000 bending cycles at a fixed bending radius of 1 mm.

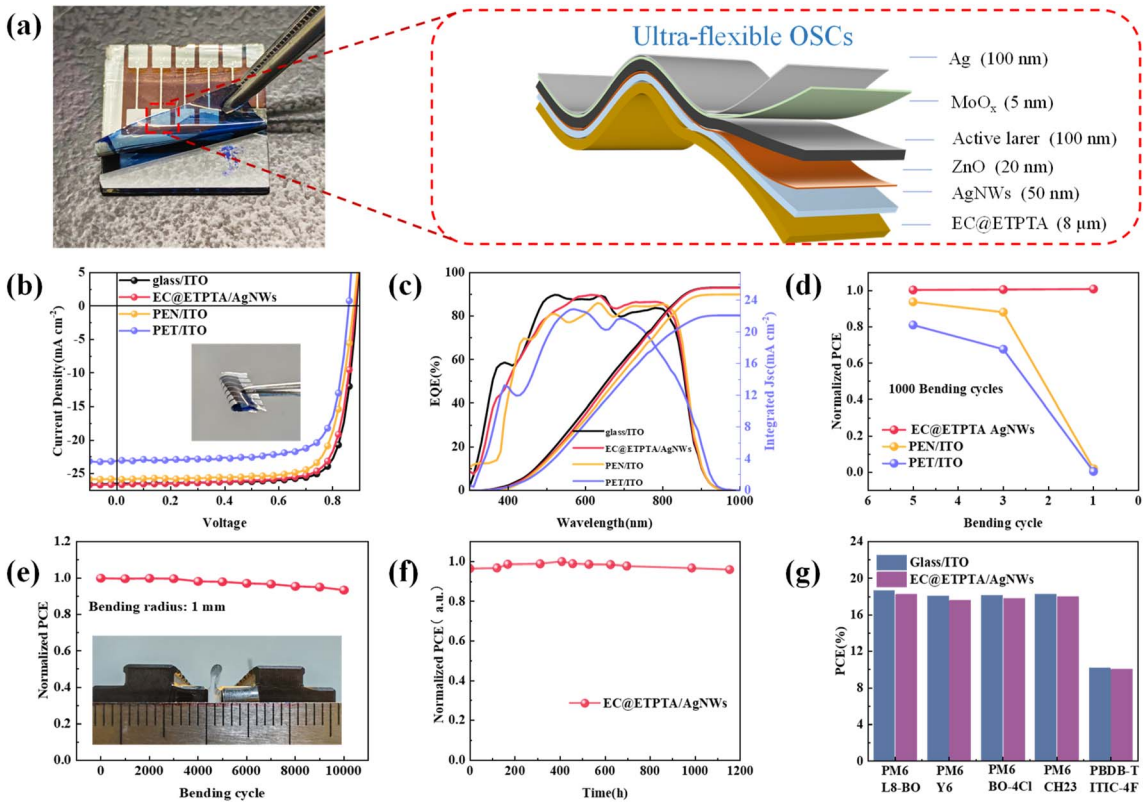

Fig. 3 (a) The device structure of the ultra-flexible OSCs based on the EC@ETPTA/AgNWs electrode. (b) *J*–*V* curves, (c) EQE spectra and the integrated J_{sc} and (d) the normalized PCE of the ultra-flexible OSCs based on EC@RTPTA/AgNWs and FOSCs based on PEN/ITO and PET/ITO after 1000 bending cycles at various bending radius. (e) The normalized PCE of the ultra-flexible device after bending cycles at a curvature radius of 1 mm. (f) Shelf storage of the ultra-flexible devices based on EC@ETPTA/AgNWs. (g) PCEs of the OSCs devices based on EC@ETPTA/AgNWs and glass/ITO electrodes with different active layer.

after bending cycles at various radii for PEN/ITO, PET/ITO, and EC@ETPTA/AgNWs-based electrodes. After 1000 bending cycles at a radius of 5 mm, the sheet resistances of all three flexible electrodes remained essentially unchanged. However, when the bending radius was reduced to 1 mm, the resistance of PEN/ITO and PET/ITO increased by 51.96 and 97.52 times, respectively, after 1000 bends. In contrast, the resistance of EC@ETPTA/AgNWs remained stable. Furthermore, as shown in Fig. 2d, the R/R_0 ratio of the EC@ETPTA/AgNWs increased only slightly to 2.07 after 10 000 bending cycles, indicating the excellent bending durability of this flexible electrode.

The excellent optoelectronic and mechanical properties of the EC@ETPTA/AgNWs electrode make it an ideal candidate for fabricating ultra-flexible organic solar cells (OSCs). We utilized this electrode to create ultra-flexible OSCs with a configuration of EC@ETPTA/AgNWs/ZnO/PM6:L8-BO/MoO_x/Ag (Fig. 3a). The detailed fabrication process is provided in the ESI.† The current density *versus* voltage (*J*–*V*) curves of the flexible device were characterized and compared to control devices based on rigid ITO on glass, PET and PEN, as shown in Fig. 3b. The photovoltaic parameters of these devices are listed in Table 1. The OSC based on glass–ITO achieved a power conversion efficiency (PCE) of 18.65% with an open-circuit voltage (V_{oc}) of 0.887 V, a short-circuit current density (J_{sc}) of 26.51 mA cm^{-2} and a fill factor (FF) of 79.41%. In comparison, the ultra-flexible OSCs achieved a PCE of 18.24%, with a V_{oc} of 0.884 V, a J_{sc} of 26.65 mA

Table 1 Photovoltaic parameters of the OSCs devices based on glass–ITO, PEN/ITO, PET/ITO and EC@ETPTA/AgNWs with PM6 and L8-BO

Electrode	V_{oc} [V]	J_{sc} [mA cm^{-2}]	J_{cal} [mA cm^{-2}]	FF [%]	PCE_{max} (PCE_{ave})[a] [%]
Glass/ITO	0.887	26.51	25.59	79.41	18.65(18.40 ± 0.24)
PET/ITO	0.858	23.11	22.08	76.04	15.10(14.54 ± 0.74)
PEN/ITO	0.877	25.81	24.72	76.42	17.30(16.73 ± 0.36)
EC@ETPTA/AgNWs	0.884	26.65	25.56	77.54	18.24(18.02 ± 0.22)
AR-EC@ETPTA/AgNWs	0.876	27.67	25.99	77.13	18.71(18.36 ± 0.44)

[a] The average PCE values were calculated from 10 devices.

Table 2 Performance parameters of the ultra-flexible devices based on EC@ETPTA/AgNWs and glass/ITO with different active layer

Electrode/ETL/active layer/HTL/Ag					
Active layer	Electrode	V_{oc} [V]	J_{sc} [mA cm^{-2}]	FF [%]	PCE$_{max}$ (PCE$_{ave}$)[a] [%]
PM6:Y6	ITO	0.847	27.43	77.71	18.06(17.60 ± 0.32)
	EC@PEGDMA/AgNWs	0.842	27.85	74.88	17.57(16.87 ± 0.85)
PM6:BO-4Cl	ITO	0.840	27.43	78.66	18.13(18.02 ± 0.24)
	EC@PEGDMA/AgNWs	0.846	27.85	75.68	17.83(17.19 ± 0.36)
PM6:CH23	ITO	0.882	26.43	78.20	18.28(18.11 ± 0.14)
	EC@PEGDMA/AgNWs	0.875	26.48	77.63	18.00(17.66 ± 0.28)
PBDBT:ITIC-4F	ITO	0.688	20.84	70.84	10.18(10.00 ± 0.34)
	EC@PEGDMA/AgNWs	0.696	20.40	70.51	10.04(9.87 ± 0.12)

[a] The average PCE values were calculated from 10 devices.

cm^{-2}, and an FF of 77.54%, which are significantly higher than those of PET and PEN-based flexible devices and represent the best-reported PCEs for flexible OSCs.

The J_{sc} values of the devices with different electrodes were further confirmed by external quantum efficiency (EQE) measurements, as shown in Fig. 3c. The EQE spectrum of the ultra-flexible OSCs exhibited higher values in the wavelength range of 550 to 850 nm compared to the control devices, which can be attributed to the high transmittance of the EC@ETPTA/AgNWs electrode.

The mechanical robustness of the ultra-flexible OSC was also evaluated under various bending conditions. Fig. 3d presents the normalized efficiencies of the ultra-flexible device, along with those of the PET/ITO and PEN/ITO-based devices, after 1000 bending cycles at different curvature radii. The PCEs of the PET/ITO and PEN/ITO-based devices decreased significantly as the radius of curvature was reduced from 5 mm to 1 mm, with the efficiencies nearly dropping to zero at a 1 mm curvature radius due to the sharp increase in resistance of the commercial flexible electrodes. In contrast, the EC@ETPTA/AgNWs-based device demonstrated exceptional flexibility and mechanical robustness, maintaining its initial efficiency even at a bending radius of 1 mm. Notably, the normalized efficiency of the ultra-flexible device only decreased by about 6.53% of its initial value after 10 000 bending cycles at a 1 mm bending radius (Fig. 3e), marking it as the best mechanical performance reported for flexible OSCs with a PCE over 18%.

Furthermore, we conducted an initial stability study of the ultra-flexible OSC. As depicted in Fig. 3f, the ultra-flexible device demonstrated excellent shelf stability, maintaining 96.04% of its initial efficiency after 1110 hours of storage in a nitrogen-filled glove box. Additionally, as shown in Fig. S13,† the device exhibited good photostability, retaining 80% of its original efficiency after 500 hours of continuous illumination at the maximum power point under 100 mW cm^{-2} LED arrays at 25 °C in a nitrogen atmosphere.

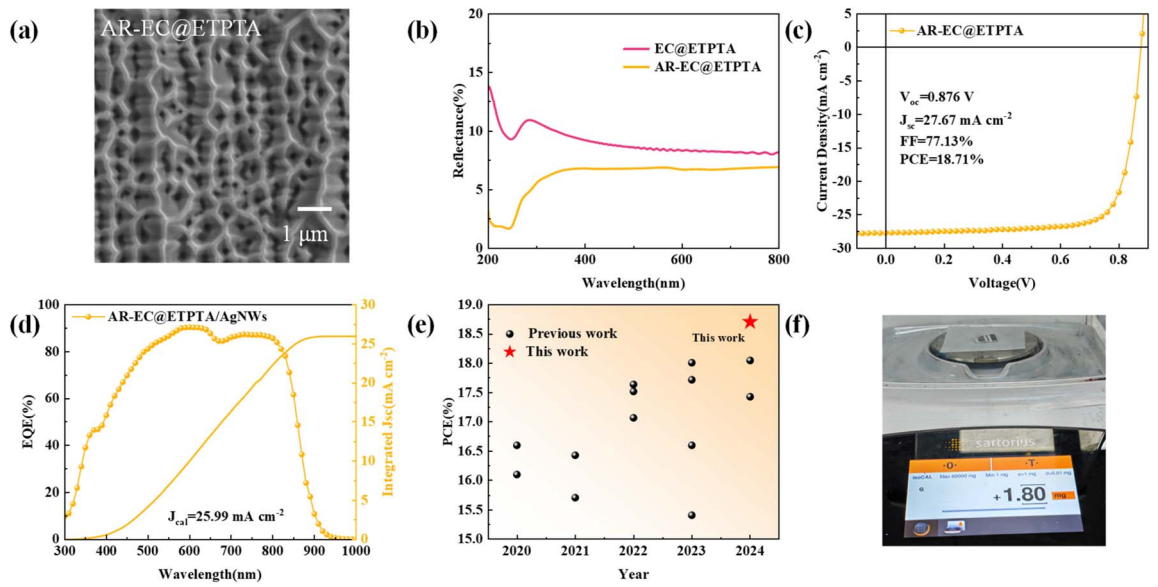

Fig. 4 (a) SEM images of the AR-EC@ETPTA film. (b) Reflection spectra of EC@ETPTA and AR-EC@ETPTA film. (c) J–V curves and (d) EQE spectra and the integrated J_{sc} of ultra-flexible device based on AR-EC@ETPTA/AgNWs. (e) Statistical diagram of PCE values obtained from the recently reported flexible OSCs. (f) Weight of the ultra-flexible device.

Building on the impressive device performance achieved with the PM6:L8BO active material, we further explored the versatility of our ultra-flexible substrate-based electrode by testing it with four other typical OSC systems (PM6:Y6; PM6:BO-4Cl; PM6:CH23 and PBDB-T:ITIC-4F, see chemical structures in Fig. S14†). As illustrated in Fig. 3g, the PCEs of the ultra-flexible devices across these different active layer material systems are comparable to those of rigid devices based on glass/ITO (Table 2 and Fig. S15†), confirming the general applicability of our ultra-flexible substrate.

To further reduce optical loss and enhance device performance, we integrated an anti-reflection (AR) structure on a silicon wafer (Fig. S16†) as a replacement for the glass substrate. The resulting AR-EC@ETPTA structure (Fig. 4a) was characterized by its reflection spectra. As shown in Fig. 4b, compared to the control film, the reflectance of the AR-EC@ETPTA substrate in the 400–1000 nm range decreased from 8.39% to 7.03%. By using this AR-enhanced composite film as the substrate for the flexible electrode and fabricating flexible devices, we achieved a high PCE of 18.71% for the PM6:L8-BO system. This improvement is attributed to the increased J_{sc} of 27.65 mA cm^{-2}, resulting from the reduced light reflection of the substrate, and marks a new record in flexible OSC efficiencies (Fig. 4e and Table S2†).

The ultra-flexible OSC device is also exceptionally lightweight. As illustrated in Fig. S17,† an ultra-flexible OSCs device was placed on a single human hair (hair from the first author) and the hair was able to support the device without deformation. As shown in Fig. 4f, the device, measuring 1.7 cm by 1.7 cm and incorporating six individual cells, weighs only 1.80 mg. This translates to a 6.23 g weight and a maximum power output of 187.15 W for a device with an area of 1 m^2. Remarkably, the ultra-flexible device achieved a power-to-weight ratio of 30.04 W g^{-1}, one of the highest reported in all photovoltaic devices. In addition, EC is non-allergenic and does not cause skin irritation, making it ideal for the development of ultra-flexible OSCs that can be worn on human skin. As demonstrated in Fig. S18,† the ultra-flexible device was attached to a finger with an irregular surface, showcasing its potential for future practical applications.

Conclusions

In summary, we have developed an eco-friendly EC-based flexible substrate by integrating UV-cured polymerization with ETPTA. The resulting composite film exhibits enhanced solvent resistance, exceptional mechanical robustness, and excellent transmittance. Utilizing this ultra-flexible substrate, we successfully fabricated ultrathin and ultra-lightweight OSCs. Notably, the PM6:L8-BO device achieved a PCE of 18.71% and a high power-per-weight ratio of 30.04 W g^{-1}, representing the best-performing ultra-flexible OSCs reported to date. Moreover, the ultra-flexible device demonstrates outstanding mechanical properties and device stability. The successful implementation of this ultra-flexible substrate and transparent electrode shows great potential for advancing flexible electronics, including OSCs.

Data availability

The data supporting this article have been included as part of the ESI.†

Author contributions

Z. Xiao carried out the flexible substrate and device fabrication and measurement. The synthesis of ZnO was conducted by J. Liu and X. Chen, Z. Suo and X. Cao contributed to part of the device measurements. X. Wan and Y. Chen supervised and directed the project. All authors discussed the results and provided feedback on the manuscript.

Conflicts of interest

There are no conflicts to declare.

Acknowledgements

The authors gratefully acknowledge the financial support from Ministry of Science and Technology of the People's Republic of China (2022YFB4200400, 2019YFA0705900, 2023YFE0210400) and National Natural Science Foundation of China (52025033, 21935007, 22361132530).

Notes and references

1 S. Xiong, K. Fukuda, K. Nakano, S. Lee, Y. Sumi, M. Takakuwa, D. Inoue, D. Hashizume, B. Du, T. Yokota, Y. Zhou, K. Tajima and T. Someya, *Nat. Commun.*, 2024, **15**, 681.
2 R. D. Andrés, R. Wessling, J. Büttner, L. Pap, A. Fischer, B. Esser and U. Würfel, *Energy Environ. Sci.*, 2023, **16**, 5255–5264.
3 Z. Li, X. Wu, S. F. Wu, D. P. Gao, H. Dong, F. Z. Huang, X. T. Hu, A. K. Y. Jen and Z. L. Zhu, *Nano Energy*, 2022, **93**, 106853.
4 J. Panidi, D. G. Georgiadou, T. Schoetz and T. Prodromakis, *Adv. Funct. Mater.*, 2022, **32**, 2200694.
5 J. W. Lee, H. G. Lee, E. S. Oh, S. W. Lee, T. N. L. Phan, S. Li, T. S. Kim and B. J. Kim, *Joule*, 2024, **8**, 204–223.
6 W. Song, Y. X. Liu, B. Fanady, Y. F. Han, L. Xie, Z. Y. Chen, K. B. Yu, X. Peng, X. L. Zhang and Z. Y. Ge, *Nano Energy*, 2021, **86**, 106044.
7 Z. Y. Wang, Y. W. Bo, P. J. Bai, S. C. Zhang, G. H. Li, X. J. Wan, Y. S. Liu, R. J. Ma and Y. S. Chen, *Science*, 2023, **382**, 1291–1296.
8 T. Yokota, I. Shirayama, K. Kuwada, M. Koizumi, W. Yukita, K. Morii, H. Fukagawa, T. Shimizu, K. Fukuda and T. Someya, *Adv. Mater. Technol.*, 2022, **7**, 2200454.
9 S. Y. Huang, Q. Z. Zhang, F. Yang, D. T. Gangadharan, P. D. Li, F. Q. Ren, B. Q. Sun and D. L. Ma, *J. Mater. Chem. A*, 2020, **8**, 8620–8628.
10 M. G. Kang, M. S. Kim, J. S. Kim and L. J. Guo, *Adv. Mater.*, 2008, **20**, 4408–4413.

11 H. H. Tang, H. R. Feng, H. K. Wang, X. J. Wang, J. J. Liang and Y. Chen, *ACS Appl. Mater. Interfaces*, 2019, **11**, 25330–25337.
12 Y. N. Zhang, J. W. Zheng, Z. Y. Jiang, X. J. He, J. Kim, L. H. Xu, M. C. Qin, X. H. Lu, A. K. K. Kyaw and W. C. H. Choy, *Adv. Energy Mater.*, 2023, **13**, 2203266.
13 Y. N. Sun, M. J. Chang, L. X. Meng, X. J. Wan, H. H. Gao, Y. M. Zhang, K. Zhao, Z. H. Sun, C. X. Li, S. R. Liu, H. K. Wang, J. J. Liang and Y. S. Chen, *Nat. Electron.*, 2019, **2**, 513–520.
14 G. Zeng, W. J. Chen, X. B. Chen, Y. Hu, Y. Chen, B. Zhang, H. Y. Chen, W. W. Sun, Y. X. Shen, Y. W. Li, F. Yan and Y. F. Li, *J. Am. Chem. Soc.*, 2022, **144**, 8658–8668.
15 Y. Sun, L. Meng, X. Wan, Z. Guo, X. Ke, Z. Sun, K. Zhao, H. Zhang, C. Li and Y. Chen, *Adv. Funct. Mater.*, 2021, **31**, 2010000.
16 B. Li, X. Yang, S. Y. Li and J. Y. Yuan, *Energy Environ. Sci.*, 2023, **16**, 723–744.
17 Z. Z. Xie, R. P. Xu, J. D. Chen, C. Li, Z. M. Bao, J. W. Zheng, Q. Sun, Y. Q. Li and J. X. Tang, *Org. Electron.*, 2019, **71**, 143–149.
18 Y. K. Zhang, S. W. Ng, X. Lu and Z. J. Zheng, *Chem. Rev.*, 2020, **120**, 2049–2122.
19 Y. Chen, Y. Y. Yue, S. R. Wang, N. Zhang, J. Feng and H. B. Sun, *Adv. Electron. Mater.*, 2019, **5**, 1900247.
20 D. Koo, S. Jung, J. Seo, G. Jeong, Y. Choi, J. Lee, S. M. Lee, Y. Cho, M. Jeong, J. Lee, J. Oh, C. Yang and H. Park, *Joule*, 2020, **4**, 1021–1034.
21 J. S. Park, G. U. Kim, S. Lee, J. W. Lee, S. Li, J. Y. Lee and B. J. Kim, *Adv. Mater.*, 2022, **34**, 2201623.
22 T. Lei, M. Guan, J. Liu, H.-C. Lin, R. Pfattner, L. Shaw, A. F. McGuire, T.-C. Huang, L. Shao, K.-T. Cheng, J. B. H. Tok and Z. Bao, *Proc. Natl. Acad. Sci. U. S. A.*, 2017, **114**, 5107–5112.
23 Y. Wang, Q. Chen, G. Zhang, C. Xiao, Y. Wei and W. Li, *ACS Appl. Mater. Interfaces*, 2022, **14**, 5699–5708.
24 J. Qin, L. Lan, S. Chen, F. Huang, H. Shi, W. Chen, H. Xia, K. Sun and C. Yang, *Adv. Funct. Mater.*, 2020, **30**, 2002529.
25 J. M. Huang, Z. Lu, J. Q. He, H. Hu, Q. Liang, K. Liu, Z. W. Ren, Y. K. Zhang, H. Y. Yu, Z. J. Zheng and G. Li, *Energy Environ. Sci.*, 2023, **16**, 1251–1263.
26 J. Kettle, A. Rees, E. B. Brousseau and M. Horie, *J. Phys. D:Appl. Phys.*, 2013, **46**, 105102.
27 K. Hashiba, S. Fujii, H. Kataura and Y. Nishioka, *IEICE Trans. Electron.*, 2016, **E99C**, 555–558.
28 X. T. Yin, P. Chen, M. D. Que, Y. L. Xing, W. X. Que, C. M. Niu and J. Y. Shao, *ACS Nano*, 2016, **10**, 3630–3636.
29 G. Zhang, Q. Chen, C. Xie, Y. Wang, C. Zhao, C. Xiao, Y. Wei and W. Li, *npj Flexible Electron.*, 2022, **6**, 37.
30 N. Y. Kwon, S. H. Park, Y. Lee, G. D. Kong, H. D. Chau, H. J. Yoon, H. Y. Woo, M. H. Hoang, M. J. Cho and D. H. Choi, *ACS Appl. Mater. Interfaces*, 2022, **14**, 34909–34917.
31 P. C. Lin, C. T. Hsieh, X. Liu, F. C. Chang, W. C. Chen, J. Yu and C. C. Chueh, *Chem. Eng. J.*, 2021, **405**, 126996.
32 L. Sun, W. Zeng, C. Xie, L. Hu and Y. Zhou, *Adv. Mater.*, 2020, **32**, 1907840.
33 Y. M. Wang, Q. M. Chen, Y. P. Wang, G. C. Zhang, Z. Zhang, J. Fang, C. W. Zhao and W. W. Li, *Macromol. Rapid Commun.*, 2022, **43**, 2200432.
34 X. Dong, P. Shi, L. Sun, J. Li, F. Qin, S. Xiong, T. Liu, X. Jiang and Y. Zhou, *J. Mater. Chem. A*, 2019, **7**, 1989–1995.
35 H. Kimura, K. Fukuda, H. Jinno, S. Park, M. Saito, I. Osaka, K. Takimiya, S. Umezu and T. Someya, *Adv. Mater.*, 2019, **31**, 1808033.
36 M. MacLeo, H. P. H. Arp, M. B. Tekman and A. Jahnke, *Science*, 2021, **373**, 61–65.
37 W. W. Y. Lau, Y. Shiran, R. M. Bailey, E. Cook, M. R. Stuchtey, J. Koskella, C. A. Velis, L. Godfrey, J. Boucher, M. B. Murphy, R. C. Thompson, E. Jankowska, A. C. Castillo, T. D. Pilditch, B. Dixon, L. Koerselman, E. Kosior, E. Favoino, J. Gutberlet, S. Baulch, M. E. Atreya, D. Fischer, K. K. He, M. M. Petit, U. R. Sumaila, E. Neil, M. V. Bernhofen, K. Lawrence and J. E. Palardy, *Science*, 2020, **369**, 1455–1461.
38 Z. P. Su, L. Cui, H. H. Zhang, L. Xiao, B. Chi, H. Y. Xu, L. P. Ning, S. S. Jia and X. H. Wang, *Chem. Eng. J.*, 2023, **471**, 144501.
39 Y. Zhou, T. M. Khan, J.-C. Liu, C. Fuentes-Hernandez, J. W. Shim, E. Najafabadi, J. P. Youngblood, R. J. Moon and B. Kippelen, *Org. Electron.*, 2014, **15**, 661–666.
40 Y. P. Xie, H. Lu, J. Huang and H. B. Xie, *Adv. Funct. Mater.*, 2023, **33**, 2213910.
41 L. B. Hu, G. Y. Zheng, J. Yao, N. A. Liu, B. Weil, M. Eskilsson, E. Karabulut, Z. C. Ruan, S. H. Fan, J. T. Bloking, M. D. McGehee, L. Wagberg and Y. Cui, *Energy Environ. Sci.*, 2013, **6**, 513–518.
42 M. Nogi, M. Karakawa, N. Komoda, H. Yagyu and T. T. Nge, *Sci. Rep.*, 2015, **5**, 17254.
43 Y. Zhou, C. Fuentes-Hernandez, T. M. Khan, J.-C. Liu, J. Hsu, J. W. Shim, A. Dindar, J. P. Youngblood, R. J. Moon and B. Kippelen, *Sci. Rep.*, 2013, **3**, 1536.
44 X. Lu, C. Xie, Y. Liu, H. Zheng, K. Feng, Z. Xiong, W. Wei and Y. Zhou, *Nat. Energy*, 2024, 1–10.
45 T. Y. Qu, L. J. Zuo, J. D. Chen, X. Shi, T. Zhang, L. Li, K. C. Shen, H. Ren, S. Wang, F. M. Xie, Y. Q. Li, A. K. Y. Jen and J. X. Tang, *Adv. Opt. Mater.*, 2020, **8**, 2000669.
46 S. A. Hashemi, S. Ramakrishna and A. G. Aberle, *Energy Environ. Sci.*, 2020, **13**, 685–743.
47 N. Alipour and H. Namazi, *Mater. Sci. Eng., C*, 2020, **108**, 110459.
48 D. F. Hou, M. L. Li, C. Yan, L. Zhou, Z. Y. Liu, W. Yang and M. B. Yang, *Green Chem.*, 2021, **23**, 2069–2078.
49 X. J. Zheng, X. L. Wu, Q. Wu, Y. F. Han, G. Y. Ding, Y. M. Wang, Y. B. Kong, T. Y. Chen, M. T. Wang, Y. Q. Zhang, J. W. Xue, W. F. Fu, Q. Luo, C. Q. Ma, W. Ma, L. J. Zuo, M. M. Shi and H. Z. Chen, *Adv. Mater.*, 2024, **36**, 2307280.
50 N. Cui, Y. Song, C.-H. Tan, K. Zhang, X. Yang, S. Dong, B. Xie and F. Huang, *npj Flexible Electron.*, 2021, **5**, 31.
51 S. Li, Z. Li, X. Wan and Y. Chen, *eScience*, 2023, **3**, 100085.
52 H. Zhang, X. Zhu, Y. Tai, J. Zhou, H. Li, Z. Li, R. Wang, J. Zhang, Y. Zhang, W. Ge, F. Zhang, L. Sun, G. Zhang and H. Lan, *Int. J. Extrem. Manuf.*, 2023, **5**, 032005.

53 M. A. Saeed, S. H. Kim, K. Baek, J. K. Hyun, S. Y. Lee and J. W. Shim, *Appl. Surf. Sci.*, 2021, **567**, 150852.
54 J. Wan, Y. Xia, J. Fang, Z. Zhang, B. Xu, J. Wang, L. Ai, W. Song, K. N. Hui, X. Fan and Y. Li, *Nano-Micro Lett.*, 2021, **13**, 44.
55 C. Xie, C. Xiao, J. Fang, C. Zhao and W. Li, *Nano Energy*, 2023, **107**, 108153.
56 D. X. Han, K. K. Zhou, X. Li, P. F. Lv, J. J. Wu, H. Z. Ke, W. C. Zhao and L. Ye, *Adv. Funct. Mater.*, 2024, 2407392.
57 X. J. Zheng, L. J. Zuo, K. R. Yan, S. Q. Shan, T. Y. Chen, G. Y. Ding, B. W. Xu, X. Yang, J. H. Hou, M. M. Shi and H. Z. Chen, *Energy Environ. Sci.*, 2023, **16**, 2284–2294.
58 J. C. Wang, L. L. Sun, S. X. Xiong, B. C. Du, T. Yokota, K. Fukuda and T. Someya, *ACS Appl. Mater. Interfaces*, 2023, **15**, 21314–21323.
59 S. Cheng, Z. Lou, L. Zhang, H. Guo, Z. Wang, C. Guo, K. Fukuda, S. Ma, G. Wang, T. Someya, H. M. Cheng and X. Xu, *Adv. Mater.*, 2022, **35**, 2206793.
60 L. S. Xie, S. Y. Du, J. Li, C. Liu, Z. W. Pu, X. Y. Tong, J. Liu, Y. H. Wang, Y. Y. Meng, M. J. Yang, W. Li and Z. Y. Ge, *Energy Environ. Sci.*, 2023, **16**, 5423–5433.
61 Z. Xiao, S. Li, J. Liu, X. Chen, Z. Suo, C. Li, X. Wan and Y. Chen, *Sol. RRL*, 2024, **8**, 2400206.
62 R. L. Shum, S. R. Liu, A. Caschera and D. A. Foucher, *ACS Appl. Bio Mater.*, 2020, **3**, 4302–4315.
63 M. Y. Yong, N. M. Sarih, S. Y. Lee and D. T. C. Ang, *React. Funct. Polym.*, 2020, **156**, 104745.
64 J. Zhong, Y. Huang, Y. Chen, L. Li and C. Guo, *Ind. Crops Prod.*, 2022, **183**, 114979.

